

## Supporting Information

### A quasi-solid-state Li-S battery with high energy density, superior stability and safety

Yi Cao, Pengjian Zuo\*, Shuailong Lou, Zhen Sun, Qin Li, Hua Huo, Yulin Ma,

Chunyu Du, Yunzhi Gao\*, Geping Yin

Figure S1

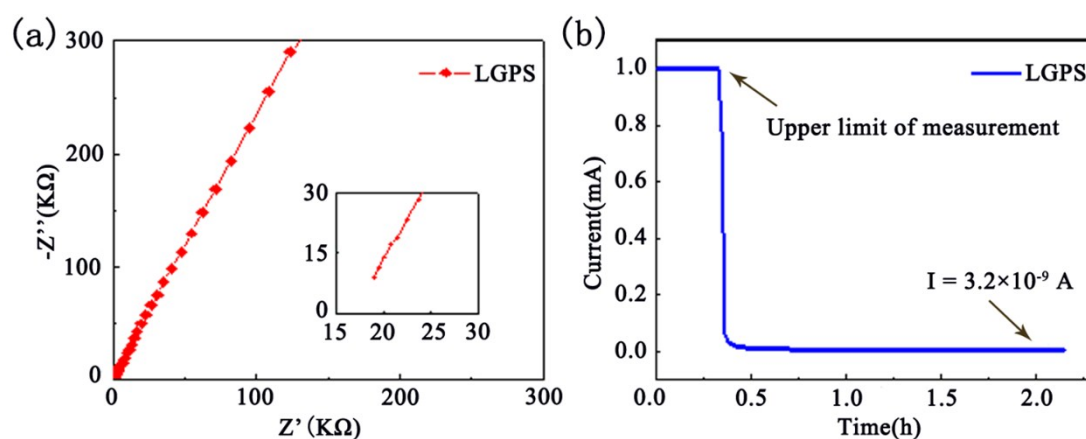


Figure. S1 the plots of (a) EIS and (b) the DC polarization measurements of the LGPS solid electrolyte

Figure. S1 shows the plots of (a) EIS and (b) the DC polarization measurements of the LGPS solid electrolyte measured under the pressure of 300 MPa. The thickness of the pellet was 1.378 mm, according to the formula

$$\sigma_{Li^+} = \frac{L}{R_s \cdot S}$$

And

$$\sigma_e = \frac{I \cdot L}{U \cdot S}$$

L, thickness of the pellet,  $L = 1.378$  mm;

S, area of the pellet,  $D = 16$  mm;

$R_s$ , the resistance obtained from EIS,  $R_s = 17.1 \Omega$ ;

I, the current obtained from DC polarization measurement,  $I = 3.2 \times 10^{-9}$  A;

U, the applied voltage,  $U = 1$  V;

The ionic conductivity and electronic conductivity of the LPS solid electrolyte were measured to be  $4.0 \times 10^{-3} \text{ S cm}^{-1}$  and  $2.2 \times 10^{-10} \text{ S cm}^{-1}$ , respectively.

**Figure S2**

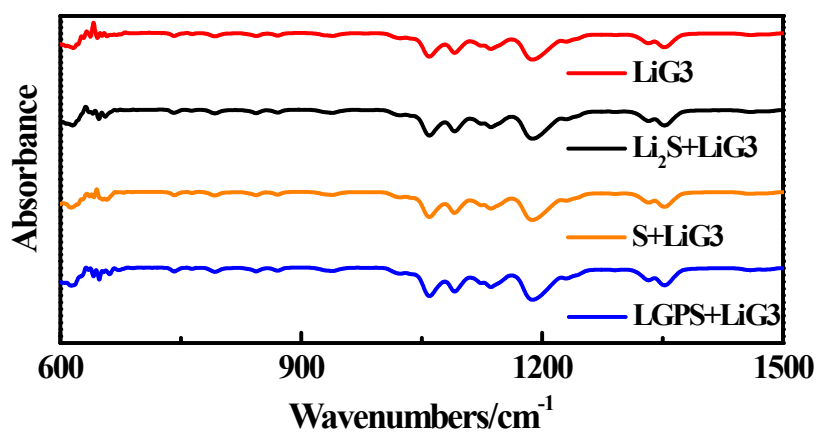


Figure. S2 IR spectroscopy of  $\text{Li}_2\text{S}$ , S and LGPS was kept with LiG3 after 30 d.

Figure. S2 shows the IR spectroscopy results of  $\text{Li}_2\text{S}$ , S and LGPS was kept with LiG3 after 30 d. The results indicates that LiG3 is no dissolving capacity and apparently reactivity with for  $\text{Li}_2\text{S}$ , S and LGPS, since the absorbance peaks are all similar to the original the absorbance peaks of LiG3.

Figure S3

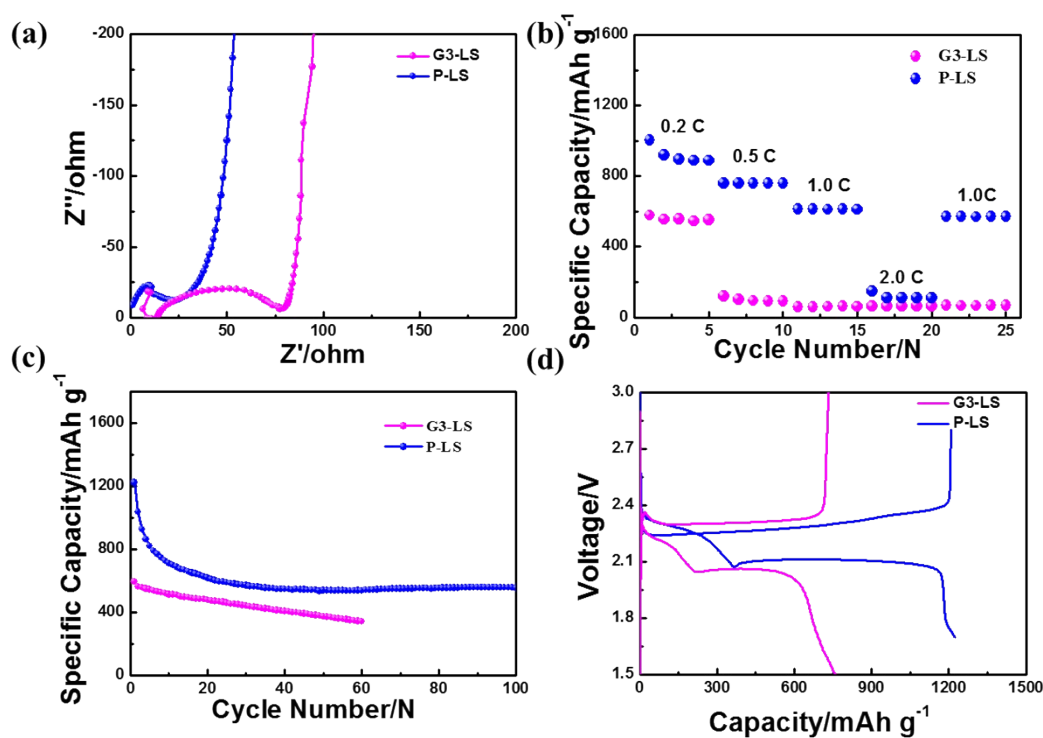


Figure. S3 (a) EIS measurements, (b) rate performances, (c) cyclic performances at 0.2 C and (d) Charge-discharge curves of G3-LS and P-LS at  $50 \mu\text{A}/\text{cm}^2$ , respectively.

Figure S4

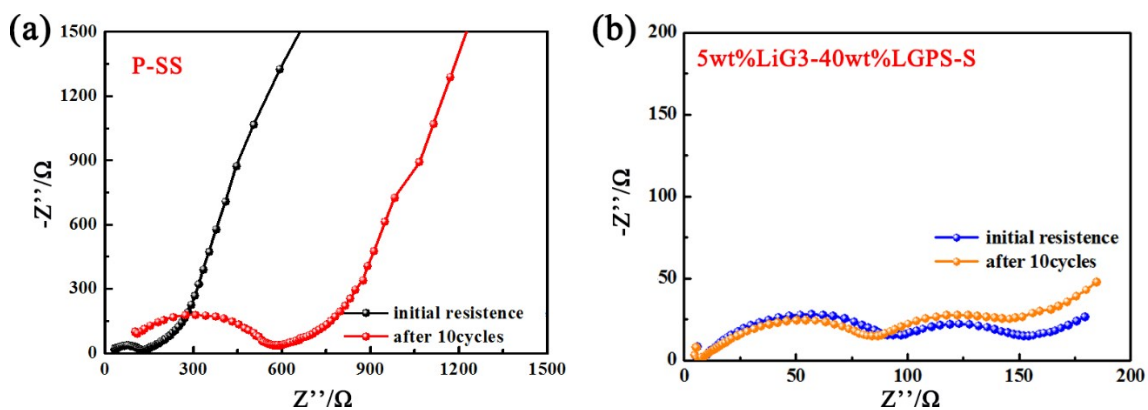


Figure. S4 EIS results of (a) P-SS and (b) 5wt%LiG3-40wt%LGPS-S before and after cycling tests.

Figure. S4 shows that charge transfer resistance of P-SS turns from  $50\Omega$  to  $300\Omega$  (Figure. S4a), by contrast, charge transfer resistance of 5wt%LiG3-40wt%LGPS-S

(Figure. S4b) keeps intact, indicating the addition of LiG3 greatly stabilizes the structure of ASS Li-S cells.

**Figure S5**

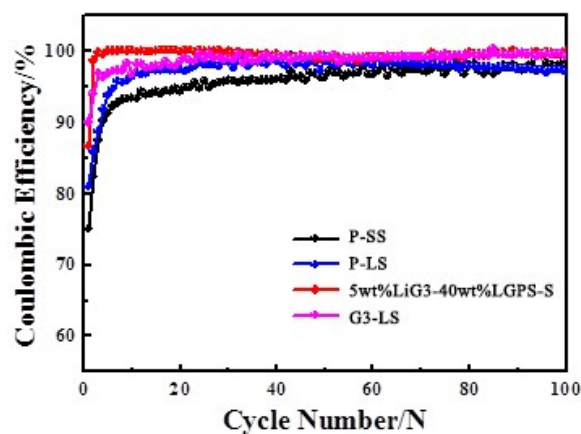


Figure. S5 Coulombic efficiency profiles of different types of Li-S batteries.

Figure. S5 presents the coulombic efficiency profiles of different types of Li-S batteries. The initial coulombic efficiency of P-LS and 5wt%LiG3-40wt%LGPS-S electrode are 81% and 87%, respectively. Moreover, the coulombic efficiency of P-LS electrode stayed between 97% and 98%, while that of 5wt%LiG3-40wt%LGPS-S electrode quickly ramp up to 100%. The coulombic efficiency of G3-LS also quickly ramp up to 100%, but the discharge capacity of G3-LS cells are only 340 mAh/g. The coulombic efficiency of P-SS is the lowest, which may be derived from the continuously side reaction between Li and LGPS interface.

**Figure S6**

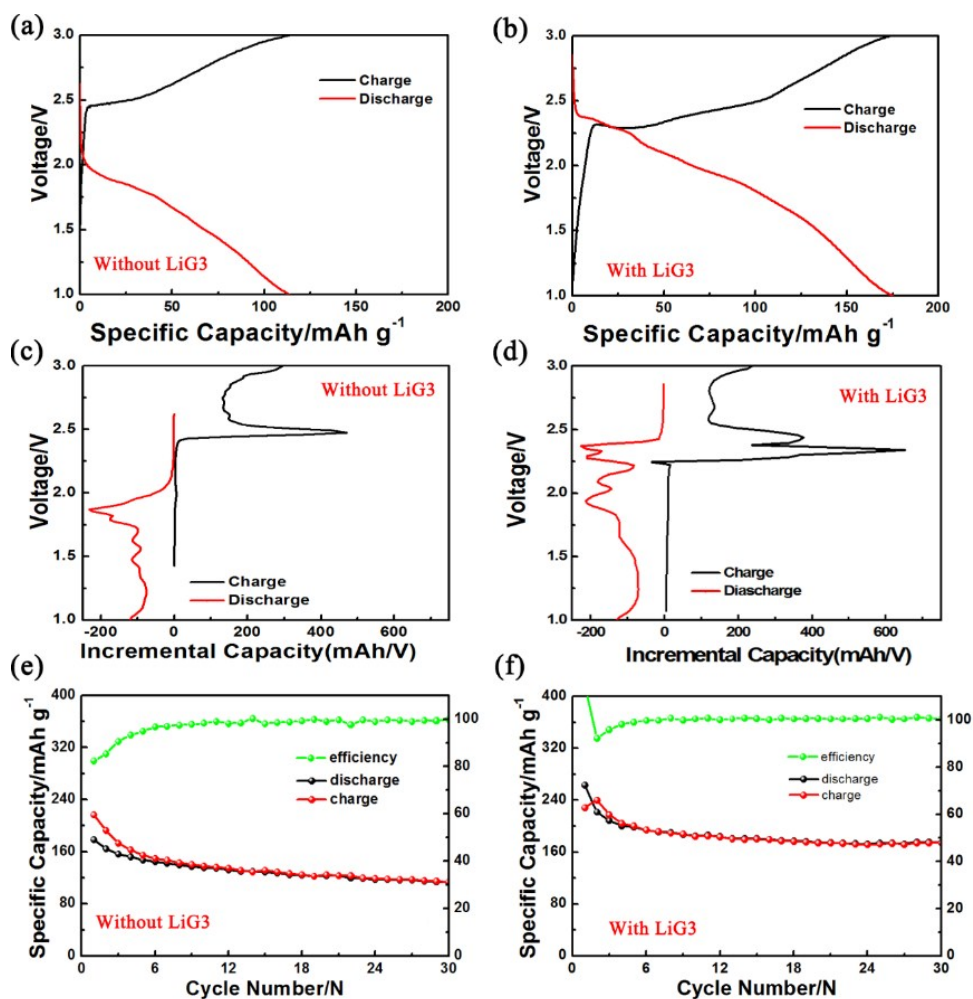


Figure. S6 (a), (b) Charge-discharge curves, (c), (d) Differential capacity curves and (e), (f) Cyclic performance of C/LGPS/C symmetric cells without LiG3 addition and with LiG3 addition, respectively.

To investigate the electrochemical stability of LGPS, C/LGPS/Li cells were assembled and tested as Figure. S6 shows. The results indicate that LGPS was decomposed and the product appears similar properties to Sulfur, whose typical charge-discharge plateau lies around 2.0 V. We further analyze the effect of LiG3 addition and find that LiG3 addition can alter the decomposition process. Moreover, according to the cyclic performance of C/LGPS/Li cells, there is no capacity growth in the following

cycles, so we think the decomposition process only occurs at the first few cycles, and the products inhibits further decomposition reaction.

**Figure S7**

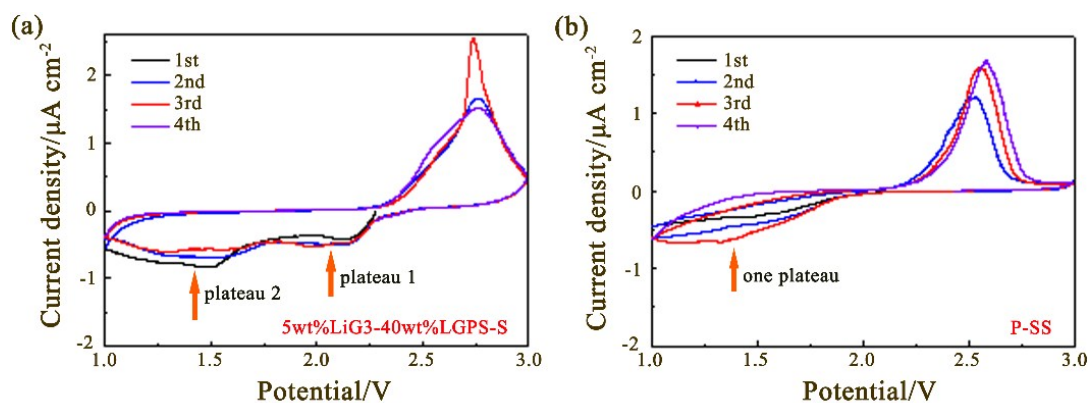


Fig. S7 cyclic voltammetry profiles of solid-state Li-S batteries with (a) 5wt%LiG3-40wt%LGPS-S and (b) P-SS electrode, respectively.

Cyclic voltammetry measurements was conducted at the scan rate of 0.1 mV/s. There exist two reductive peaks at 1.5 V and 2.1 V, respectively in the 5wt%LiG3-40wt%LGPS-S electrode, while there is only one reductive peaks at 1.5 V. The reductive potential measured by CV is slight deviation from the discharge-charge curves, which may be derived from the faster scan rate.

**Figure S8**

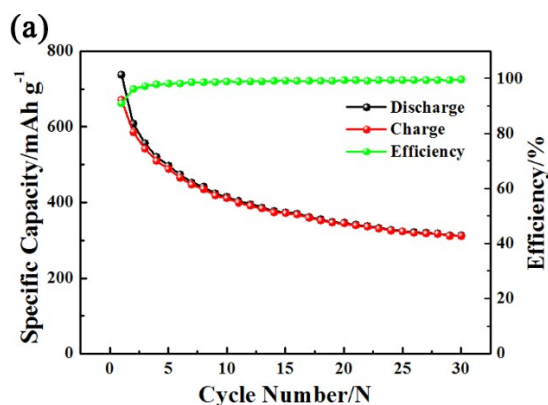


Figure. S8 Cyclic performance of Li-S cells 45wt%LiG3-S at 0.2 C, RT.

Cells 45wt%LiG3-S: There is only LiG3 in cathode side, SE layer was LGPS pellet and Li metal acts as anode. Cathode was prepared by normal coating method with mass ratio of S:C<sub>KB</sub>:PVDF = 8:1:1.

**Figure S9**

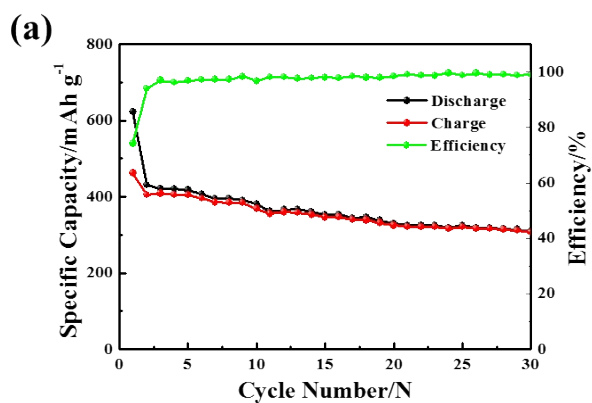


Figure. S9 Cyclic performance of Li-S cells 5wt%LiG3-40wt%SiO<sub>2</sub>-S.

Cells 5wt%LiG3-40wt%SiO<sub>2</sub>-S: Cells 5wt%LiG3-40wt%SiO<sub>2</sub>-S were fabricated by the similar process of 5wt%LiG3-40wt%LGPS-S, here we replace LGPS with SiO<sub>2</sub> (30 nm, Aladdin) within the cathode 5wt%LiG3-40wt%LGPS-S, which is Li<sup>+</sup> insulation.

**Figure S10**

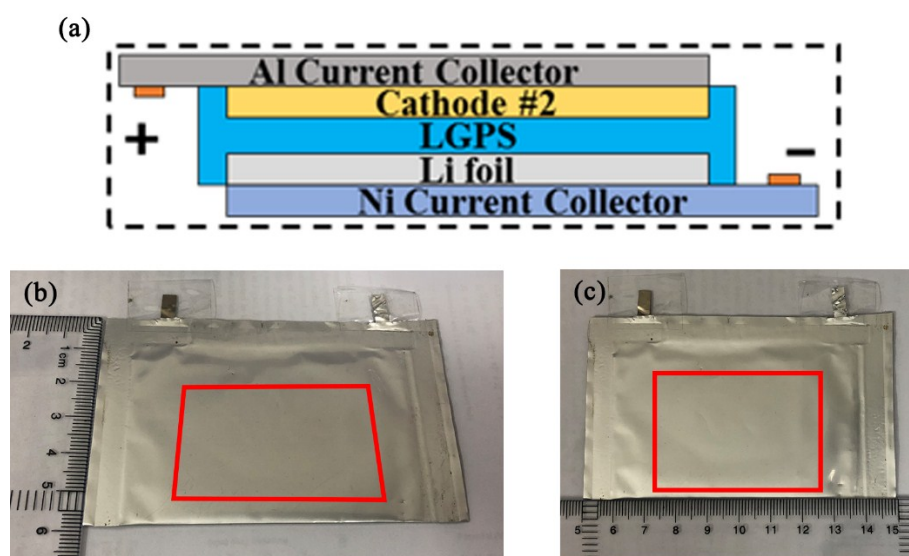


Figure. S10 (a) Schematic diagram representing structure of pouch cell, (b) and (c) Photographic images of solid-state Li-S pouch cell fabricated by coating method (dimension information), red rectangle represents real electrode size in pouch cell.

Figure. S10a illustrates the structure of pouch cell, the cathode was fabricated by coating method as we reported before,<sup>1</sup> the composite cathode targeted weight ratio of sulfur, LGPS electrolyte, VGCFs, LiG3 complex and polybutadiene (act as binders) is 4: 2: 2: 0.5: 0.3. SE layer was also fabricated by coating method with 3% polybutadiene addition. Figure. S10b and S10c present the actual length and width of the pouch cell (red tetragon), respectively.

**Table S1**

Table S1. Latest published data for solid-state Li-S batteries.

SE	Capacity (mAh g <sup>-1</sup> S)	S loading (mg cm <sup>-2</sup> )	Current density	Cycles N	Ref.
Li <sub>6</sub> PS <sub>5</sub> Br	1200	0.46	167 mA g <sup>-1</sup>	50	2
Li <sub>6</sub> PS <sub>5</sub> Cl	500	0.6	64 μA cm <sup>-2</sup>	20	3
Li <sub>9.54</sub> Si <sub>1.74</sub> P <sub>1.44</sub> S <sub>11.7</sub> Cl <sub>0.3</sub>	800	0.3	80 mA g <sup>-1</sup>	60	4
Li <sub>7</sub> P <sub>2.9</sub> Mn <sub>0.1</sub> S <sub>10.7</sub> I <sub>0.3</sub>	800	-	0.05 C	60	5
Li <sub>10</sub> GeP <sub>2</sub> S <sub>12</sub> + 75Li <sub>2</sub> S-24P <sub>2</sub> S <sub>5</sub> - P <sub>2</sub> O <sub>5</sub>	800	0.5	0.05 C, 60°C	30	6
70Li <sub>2</sub> S-30P <sub>2</sub> S <sub>5</sub>	500	0.4	44 μA cm <sup>-2</sup>	10	7
Li <sub>10</sub> GeP <sub>2</sub> S <sub>12</sub>	1000-1100	0.5-1.2	0.2 C	100	This work
	650		1.0 C	500	

**References**

1. Y. Cao, Q. Li, S. Lou, Y. Ma, C. Du, Y. Gao and G. Yin, *Journal of Alloys and Compounds*, 2018, **752**, 8-13.
2. M. Chen and S. Adams, *Journal of Solid State Electrochemistry*, 2014, **19**, 697-702.
3. C. Yu, L. van Eijck, S. Ganapathy and M. Wagemaker, *Electrochimica Acta*, 2016, **215**, 93-99.
4. R. Xu, Z. Wu, S. Zhang, X. Wang, Y. Xia, X. Xia, X. Huang and J. Tu, *Chemistry - A European Journal*, 2017, **23**, 13950-13956.
5. R.-c. Xu, X.-h. Xia, S.-h. Li, S.-z. Zhang, X.-l. Wang and J.-p. Tu, *Journal of Materials Chemistry A*, 2017, **5**, 6310-6317.
6. X. Yao, N. Huang, F. Han, Q. Zhang, H. Wan, J. P. Mwizerwa, C. Wang and X. Xu, *Advanced Energy Materials*, 2017, **7**, 1602923.
7. Y. Zhang, K. Chen, Y. Shen, Y. Lin and C.-W. Nan, *Solid State Ionics*, 2017, **305**, 1-6.